PAPER

Characterizing seasonal recharge between a river and shallow aquifer in a floodplain based on time-lapse electrical resistivity tomography

Yongshuai Yan[1] · Yaping Deng[1] · Lei Ma[1] · Guizhang Zhao[2] · Jiazhong Qian[1]

Abstract

Recharge between a river and shallow aquifer in a floodplain involves critical hydrological processes for the whole ecological environment, which often exhibits heterogeneity because of seasonality and geological complexity. In this study, electrical resistivity tomography (ERT) was used to analyze the temporal and spatial variations in the recharge characteristics of a floodplain under a variety of climatic and geological conditions. Two sets of ERT tests (in the dry season and wet season) were conducted. Each test included four ERT lines to capture the dynamic electrical resistivity distribution associated with season-driven, river and shallow groundwater interactions along a stretch of the Yellow River (adjacent to the floodplain) in China. The findings indicate that this floodplain is composed of three distinct hydrogeological units. Additionally, ERT images taken during the wet season demonstrate that river water recharges the shallow aquifer and then flows toward the middle aquifer via several seepage channels. Based on time-lapse ERT images, different recharge characteristics are identified in the low and high floodplain. In the low floodplain, both the Yellow River and the vadose zone are preferential shallow groundwater recharge zones. In the high floodplain plain, only the vadose zone is a preferential shallow groundwater recharge zone. Resistivity mapping can provide valuable information about the recharge between surface-water bodies and shallow aquifers. This is particularly useful when combined with water level data, and resistivity distribution with depth can also be used to characterize the stratigraphic structure of the floodplain.

Keywords Seasonal recharge · Electrical resistivity tomography · Hydrogeological units · Floodplain · Arid regions · China

Introduction

In many parts of the world, shallow aquifers constitute the primary source of freshwater (Hiscock and Grischek 2002; Levy et al. 2011). To meet the growing demand for freshwater, shallow aquifers need to be recharged. Shallow aquifer recharge is a crucial hydrological process in which water from a river or rainfall enters a shallow aquifer where it is then stored as groundwater. The recharge relationships between a river and shallow aquifer are usually controlled by the local hydrogeological structure (Fleckenstein et al. 2006; Ward et al. 2010a, b; Krause et al. 2012; Kumar 2018). However, the spatial distribution of sediment structural heterogeneity cannot be measured well, which increases uncertainty about the sustainability of groundwater resources in arid and semiarid areas (Storey et al. 2003; Cardenas et al. 2004; Weatherill 2015). Hence, these relationships are significantly variable in space and time. A basic understanding of the recharge relationships between the river and the shallow aquifer is crucial for improved conservation and for the development of shallow aquifer resources.

Traditional methods, such as pumping tests (Satter and Keramat 2016), slug tests (Bingly et al. 2013; Sebok et al. 2015) and permeameter testing (Cheng et al. 2011), are commonly employed to characterize the heterogeneity of the hydrogeological structure. However, the full characterization of a shallow aquifer at a large spatial scale often requires many observation wells because of the heterogeneity of natural aquifers, which may be unaffordable and operationally inefficient (Gelhar 1986). The tracer test method (Harvey

✉ Guizhang Zhao
zhaoguizhang@ncwu.edu.cn

✉ Jiazhong Qian
qianjiazhong@hfut.edu.cn

[1] School of Resources and Environmental Engineering, Hefei University of Technology, Hefei 230009, China

[2] School of Earth Geosciences and Engineering, North China University of Water Resources and Electric Power, Zhengzhou 450045, Henan, China

and Bencala 1993; Constantz 2008; Swanson and Cardenas 2010; Xie and Batlle-Aguilar 2017; Zhang et al. 2017; Zhou et al. 2017; Liu et al. 2018; Yang et al. 2021) is an indirect approach, averaged over larger volumes. Therefore, it fails to identify spatial structure heterogeneity, such as areas of high and low subsurface mobility (Singha et al. 2008; Foster et al. 2021).

Over the past several decades, geophysical approaches have been extensively used to define aquifer structural characteristics, determine aquifer material, and map environmental pollution (Binley et al. 2015; Hermans et al. 2014; Singha et al. 2015). Electrical resistivity tomography (ERT) is one of the most often used geophysical methods for hydrogeological studies. ERT, a promising approach for mapping the groundwater and surface-water interaction zone and its dynamics where both have a suitable electrical current contrast, is conducted by injecting electrical currents into the ground via two electrodes and measuring the resultant voltage between two additional potential electrodes (Cardenas et al. 2010; Bingly et al. 2015). It is a well-developed technique for volumetric imaging of temporal hydrological processes (Musgrave and Binley 2011). In comparison to other geophysical methods, ERT provides a continuous monitoring profile rather than a series of isolated points (Binley 2015; Singha et al. 2015).

The time-lapse ERT method is a significant technique for measuring solute transport. For example, it has been used to conduct salt tracer experiments (Singha and Gorelick 2006; Singha et al. 2007; Wilkinson et al. 2010) and monitor heat transport (Revil et al. 1998; Rein et al. 2004; Hayley et al. 2007; Ludwig and Hession 2015). ERT has also been used for characterizing saline intrusion in shallow coastal aquifers (Acworth and Timms 2003; Maurer et al. 2009; Nguyen et al. 2009; Ogilvy et al. 2009; Sutter and Ingham 2017; Yeh et al. 2008) and for mapping contaminant migration (Deng et al. 2017); (Nimmer et al. 2007; Slater and Binley 2006). Most time-lapse ERT experiments have aimed to improve understanding of subsurface solute transport by using time-varying electrical resistivity associated with heat or saline tracer techniques in groundwater; however, few studies have explored the interaction between river water and groundwater utilizing ERT imaging and river water tracing (a natural tracer method) in a large river.

River water tracing may uncover valuable underground information and has received widespread interest because of its low environmental impact compared to standard tracing methods. Ward et al. (2010a, b) used two-dimensional (2D) ERT imaging in conjunction with stream tracers to identify a dynamic-hyporheic zone at spatial and temporal scales as did Nyquist et al. (2008) in their approach to describe the zone of aquifer seepage into rivers at various stages. Coscia et al. (2011) characterized an aquifer and monitored infiltrating river water by using the three-dimensional (3D)

ERT method, whereas Johnson et al. (2015) investigated stage-driven river water intrusion using four-dimensional (4D) ERT monitoring. The obtained findings demonstrated that electrical resistivity is very sensitive to water level changes. Further research used time-lapse ERT to characterize groundwater recharge on the same vadose zone over various periods; however, time-lapse ERT has not been utilized to characterize two geologically contrasting vadose zones within the same season. The properties and processes of rivers and shallow aquifers are spatially and temporally highly heterogeneous. Heterogeneity in alluvial deposits can influence permeability. Sediment heterogeneity also affects hyporheic exchange, which refers to surface water entering and flowing within streambed sediments over scales from centimeters to tens of meters before it discharges back into the stream (Lautz and Siegel 2006). Despite the importance of heterogeneity, streambed sediments are not typically characterized at small scales, although novel technology for such small-scale characterization is being explored (Kelly and Murdoch 2003); furthermore, few studies have explored the recharge relationships between the river and the shallow aquifer across different orders of streams (Kiel and Bayani Cardenas 2014; Marzadri et al. 2017). To fill these gaps, a time-lapse ERT method is required that provides spatially and temporally complete data sets about geological and hydrological information at the site (Harvey and Gooseff 2015; Hester et al. 2017; Ward 2016).

The purpose of this work is to increase understanding of the recharge interaction between rivers and shallow aquifers by combining time-lapse ERT with hydrological data. Seasonal fluctuations in resistivity in the vadose zone and shallow aquifer assist in analyzing the recharge connection between the river and shallow aquifer. The first objective of this study is to identify the distribution of the vadose zone, shallow aquifer and middle aquifer at a suitable site, as well as their associated resistivity. The second objective is to analyze seasonal fluctuations in groundwater recharge of the vadose zone in high and low floodplains and to assess the river's involvement in shallow aquifer recharge.

Materials and Methods

Site description

The research site is situated along the section of the Yellow River approximately 9 km south of downtown Yuanyang in Henan province, China (Fig. 1a). In the study zone, the Yellow River, a flat area with an elevation ranging from 83 to 86 m above mean sea level, is about 0.8 km wide and 10 m deep. The water of the Yellow River is inextricably related to groundwater and replenishes a porous sandy aquifer on a continuous basis (Peng et al. 2010). Regarding its climatic
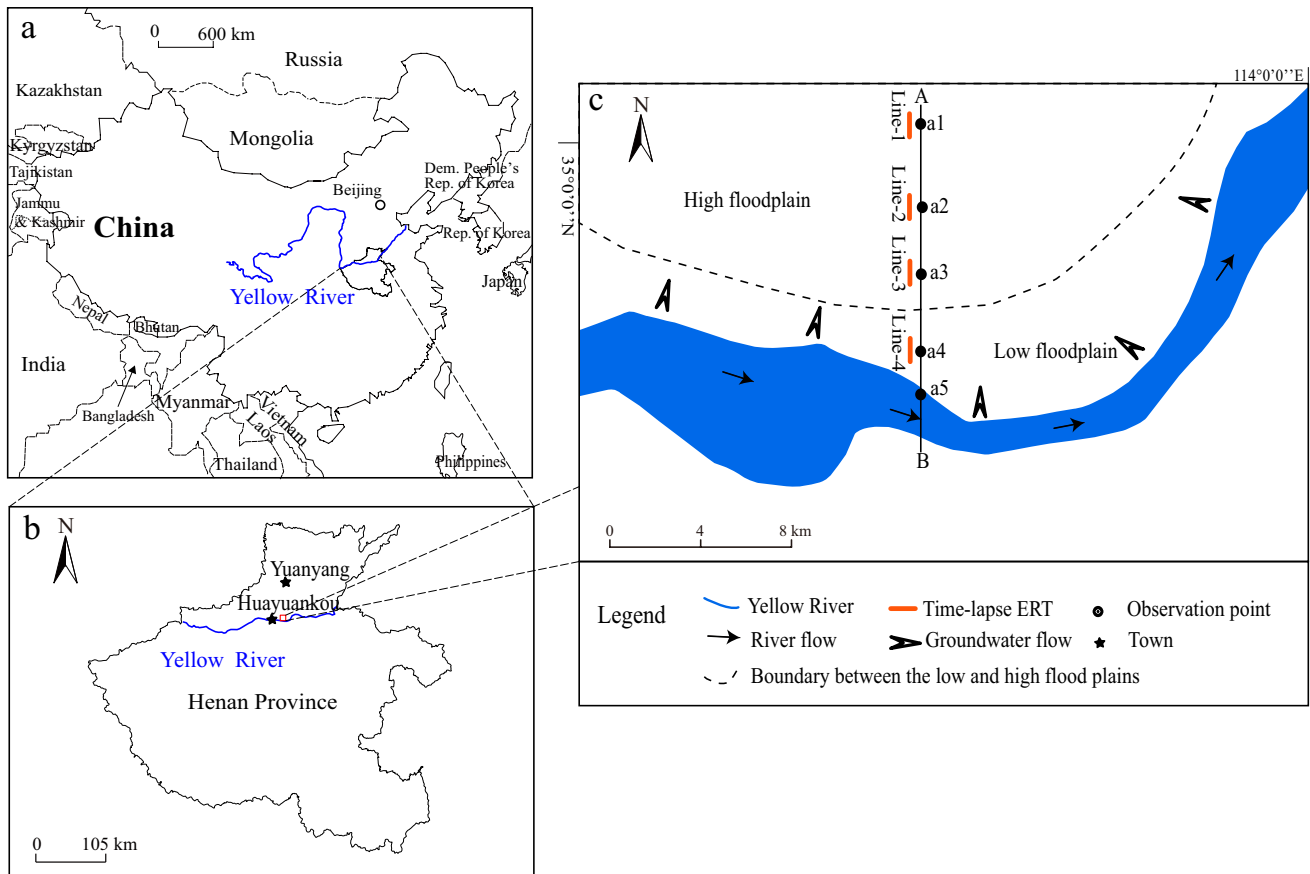
Fig. 1 Overview map of the study area illustrating the locations of electrical resistivity tomography (ERT) measurement lines and observation points. **a** Map of China, where the highlighted black line indicates Henan province and the blue line is the Yellow River. **b** Henan province, where the red box indicates the location of the study region. **c** ERT survey lines, observation points, and recharge section (A–B)

characteristics, the region is moderately cold in winter and warm in summer, indicative of the ocean monsoon climate; furthermore, the area generally has relatively humid climate and mild temperatures (average temperatures of 12–14 °C; Wohlfart et al. 2016). Available precipitation data indicate that the monthly average precipitation was 12.9 mm in December 2018, while in June 2019, it was 111.5 mm (data sourced from Yellow River Conservancy Commission of the Ministry of Water Resources). Figure 2 shows the rainfall and temperature data for the research zone from January 2018 to September 2019.

Morphologically, this area is part of the Yellow River basin and has characteristics typical of the floodplain geomorphology. The formation of floodplains is associated with flood activity. As the frequency of floods has varied, multiple floodplains caused by floods during different periods exist simultaneously on the same river. These floodplains are divided into high and low floodplains according to their elevation (Liu et al. 2019). Figure 3 shows the general location and geological maps of the study area. Because the low floodplain zone is closer to the riverbed and formed later, it

is covered by a sequence of alluvial sediments consisting of sandy silt, sand, and silty clay, with a well-developed aquifer linked directly to the Yellow Riverbed. The ERT survey line 4 and monitoring well a4 are distributed within the low floodplain. In contrast, the high floodplain was formed in an earlier period and is far from the riverbed, characterized by the strata system of silty clay and sand. The other three ERT lines and three monitoring wells are distributed within the high floodplain. More details about the geology of this area are presented in the following section.

Geologically, the study area consists of Holocene series (Q_h^{a1}) and upper Pleistocene alluvium (Q_p^{3a1}). Holocene series alluvium is distributed at a depth of 0–8 m and composed of silty clay (high floodplain) and sandy silt (low floodplain). Upper Pleistocene alluvium is distributed at a depth of 8–72 m, and mainly consists of sand and sand with silty clay. A geological cross-section is shown in Fig. 3. Groundwater is found in both the shallow aquifer and middle aquifer, which occur in the upper Pleistocene alluvium. The thickness of the shallow aquifer is about 11 m, the water-table depth of the shallow aquifer is about 8 m,

Fig. 2 Precipitation and air temperature data for the period from January 2018 to September 2019
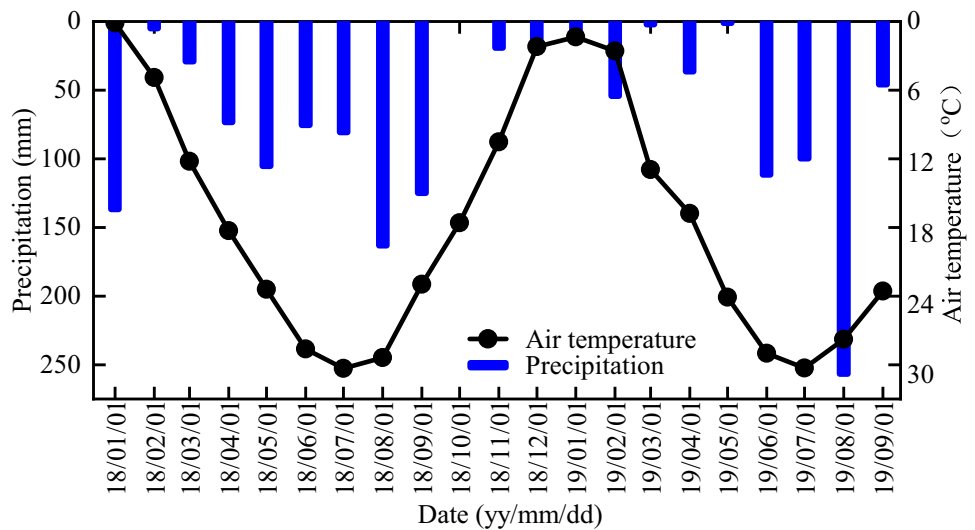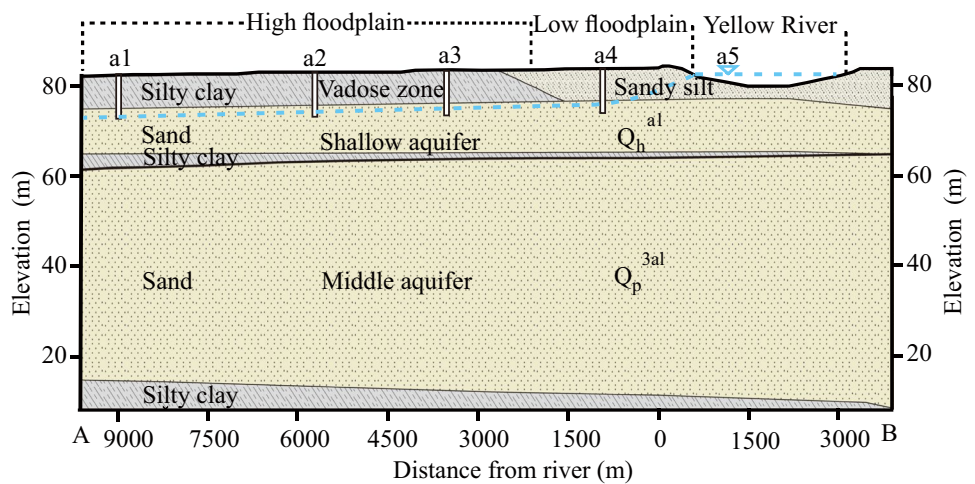

Fig. 3 Geological cross-section along A–B (see Fig. 1)

and the groundwater general flow direction is from south to north. This shallow aquifer has a moderate to high erosion potential and is mostly recharged by the Yellow River, as it is a suspended river beginning at Huayuankou (Yu 2002). The middle aquifer is separated from the shallow aquifer by a thin layer of silty clay. The thickness of the middle aquifer is about 45 m. In this region, the varied deposition of the meandering Yellow River results in high lithologic heterogeneities in the shallow aquifer and middle aquifer. Both aquifers are the primary water source for agricultural irrigation and residential water use.

Electrical resistivity tomography

The ERT method is based on Ohm's law. Bulk electrical resistivity (ρ_b) is defined as the ratio of the potential difference (ΔV) to the current intensity (I) multiplied by the electrical resistivity coefficient (K) of the device. The electrical

resistivity value was determined using Eq. (1) (Yang et al. 2021):

$$\rho_b = K \frac{\Delta V}{I} \tag{1}$$

ERT was utilized to determine the potential differences between electrodes M and N by supplying current I at the ground surface from opposing electrodes A and B. Furthermore, the coefficient of the device was calculated according to Eq. (2):

$$K = \frac{2\pi}{\frac{1}{AM} - \frac{1}{AN} - \left(\frac{1}{BM} - \frac{1}{BN} \right)} \tag{2}$$

where K represents the coefficient of the device, and AM, AN, BM, and BN represent the distances between electrodes.

In this experiment, ERT data were collected using DUK-2B (CGE Geological Instrument Company Limited, China). A Wenner Alpha electrode configuration array

was employed because it has the strongest signal strength, which is an important factor as the investigation was conducted in a groundwater system that was expected to present background noise (Loke 2004; Sutter and Ingham 2017). Effective time-lapse imaging generally requires that noise conditions remain invariant over time. In many cases, noise levels can be estimated by collecting repeat and reciprocal measurements during quiescent conditions prior to a certain expected event. In this case, however, there were no such quiescent conditions because of the fluctuating river stage and water table, which made it problematic to differentiate between data variability caused by background noise and data variability caused by the fluctuating water table. Therefore, noise levels were reduced using the Wenner Alpha electrode configuration array, a collection configuration which offers high vertical and horizontal resolutions and a low signal-to-noise ratio. Before collecting ERT data, a good flow of electrical current into the subsurface was confirmed by low values of contact resistance (less than 1 KΩ), measured between the electrode and the ground. Preliminary electrical data were collected to set transmission parameters such as the injected current and potential measured. The duration of the injection pulse was 250 ms, while the minimum and maximum number of cycles for each measurement were 3 and 6, respectively. The measurement time was set to 2 s, and the standard deviations of all channels were less than 2%.

Data from the 2D ERT were inverted using EarthImager 2D inversion software developed by Advanced Geosciences Incorporated (Loke and Barker 1996). In this study, the least squares inversion method (L2) was chosen as the inversion model for the measured resistivity value because of the model roughness (Kim et al. 2009). This model applies the L2 norm and minimizes the sum of squares of the spatial changes in model resistivity and data misfits. Then, the inversion minimizes the root mean square error between the measured and inverted resistivity values. The inversion progress was set to stop when the root mean square error between the measured and calculated apparent resistivity values reached less than 5% (implying convergence of the inversion). Finally, two periods of ERT images, one for each monitored plot, were inverted independently. A robust smoothness constraint option (Claerbout and Muir 1973), which minimizes the absolute changes in the model resistivity values, was applied. In the present study case, time-lapse ERT inversion was carried out using dry season datasets as the base model (background data) for the wet datasets recorded later. The output is presented as percentage change in the resistivities from the base model. To identify the hydrogeological units and assess the influence of river seepage on the shallow aquifer, DUK-2B was used to collected ERT data twice—once on December 14, 2018, during the dry season, and once on June 6, 2019, during the wet

season. With increasing distance from the Yellow River, four ERT lines were drawn from south to north and perpendicular to the Yellow River course, where the first ERT line is 9 km away from the edge of the Yellow River (Figs. 1c and 5). The length of these ERT lines was 354 m and 60 electrodes were used with 6 m of spacing between them. These ERT lines, oriented from north to south, were fixed over the time-lapse ERT investigation period to monitor the variation of resistivity values over time (Fig. 4). During the measurement, ERT parameters were the same for each measurement, as shown in Table 1.

As ERT imaging is conducted repeatedly at the same location, any variations in resistivity are mostly caused by changes in pore-water resistivity (effectively, in the chemistry of the water) or bulk temperature (Archie 1942). The contributions of changing groundwater temperature to resistivity were analyzed first. During installation of the well, temperature loggers (Suzhou Nanzee Sensing Technology Co., Ltd., China) were buried in sediments at depths of 12 m (each sensor probe is 1 m long) below the ground surface to monitor the actual temperature profile.

The temperature profiles in the subsurface soil (from a depth of 1–12 m) obtained for both the surveying campaigns of this study are shown in Fig. 5. It is important to note that the upper part of the subsurface was influenced by both the wet and dry seasons. In the wet season, the temperature in the subsurface soil decreases with increasing depth, while the reverse is true for the dry season. Although air temperature differs significantly between the dry season and the wet season, the temperature in the subsurface soil tends to approximate the annual average temperature of 14 °C (Amabile et al. 2020; Nijland et al. 2010). Below a depth of 8 m, small temperature variations were observed in the subsurface soil, and any variations in bulk resistivity can be attributed to variations in pore fluid resistivity. The ratio between the pore fluid resistivity (ρ_f) and the bulk resistivity (ρ_b) is known as the formation factor (F), which is defined as $F \times \rho_f = \rho_b$ (Archie 1942). The pore fluid resistivity can be used to characterize the type of fluid in the subsurface soil at a specific location. If the pore fluid resistivity is known (e.g., from conductivity measurements in wells), the formation factor (F) can be approximated for the hydrogeological units on a bulk resistivity image (Sutter and Ingham 2017).

Hydrological monitoring well

Five hydrological monitoring wells (a1–a5) were dug to further examine the distribution and structure of the shallow aquifer and to collect data on lithology. The purpose of the existing wells was extended to also monitor the level of both the groundwater and the Yellow River water. The exact locations of the wells are shown in Fig. 1c. Well a1 is located near ERT line 1 (approximately 9 km north of

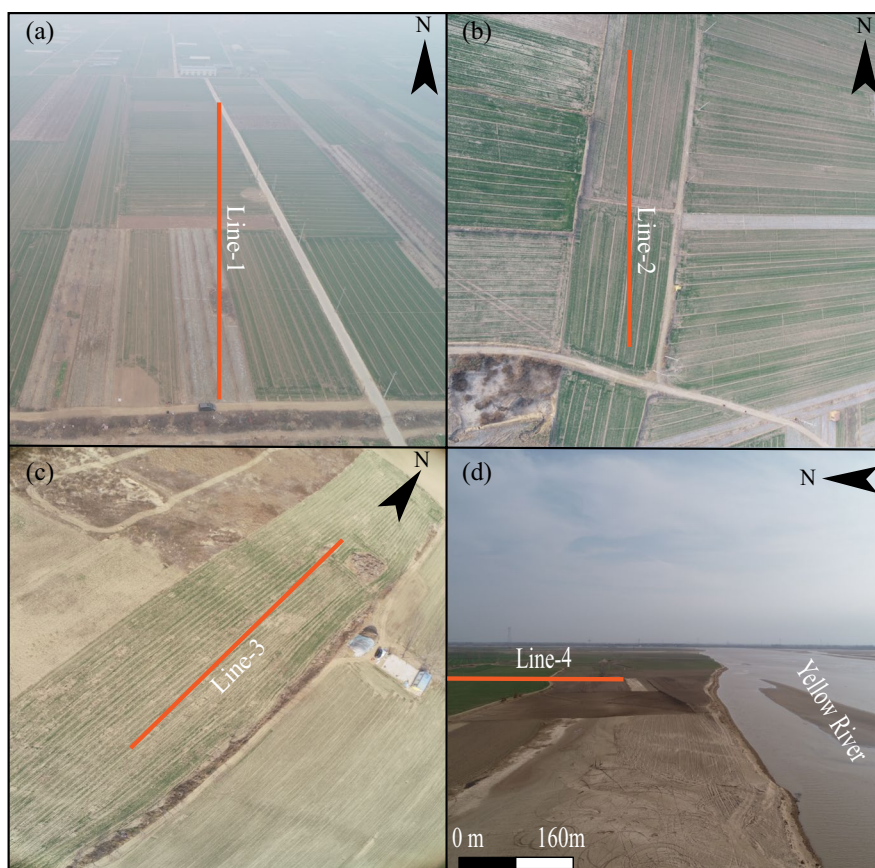**Fig. 4** ERT transects of **a** line 1, **b** line 2, **c** line 3, and **d** line 4

Table 1 Electrical resistivity tomography (ERT) settings for the sites

Line ID	Orientation	Distance from the river (km)	Electrode spacing (m)	Electrode No.	Length (m)	Measurement date
1	S–N	9	6	60	354	14 Dec. 2018
1	S–N	9	6	60	354	6 Jun. 2019
2	S–N	5.8	6	60	354	14 Dec. 2018
2	S–N	5.8	6	60	354	6 Jun. 2019
3	S–N	3.45	6	60	354	14 Dec. 2018
3	S–N	3.45	6	60	354	6 Jun. 2019
4	S–N	1.2	6	60	354	14 Dec. 2018
4	S–N	1.2	6	60	354	6 Jun. 2019

the Yellow River) on the high floodplain, while well a2 is situated near ERT line 2 (approximately 5.8 km north of the Yellow River) on the high floodplain. At 3.45 km north of the Yellow River, well a3 is located on the high floodplain near ERT line 3, whereas well a4 is situated along ERT line 4 (approximately 1.2 km north of the Yellow River) on the low floodplain, and well a5, used for monitoring the water level of the Yellow River, is located on the Yellow River bed. The other wells (a1, a2, a3, and a4) were used for long-term monitoring of the water table of the shallow

aquifer. Both the water level in the wells and the water level of the Yellow River were measured with electronic pressure sensors (Rugged Troll 100, IN-situ Inc. USA), whereby the water level and river stage were recorded at an interval of 1 day.

Groundwater samples from wells a1–a4 and river water samples from well a5 (Fig. 1c) were collected both in December 2018 and June 2019. Electrical conductivity (EC) levels of both groundwater and river water are summarized in Table 2. The groundwater EC was always lower than the river EC.
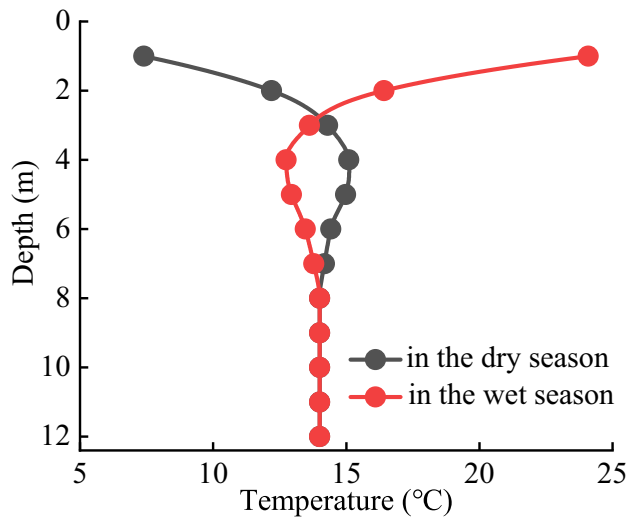
Fig. 5 Temperature in the subsurface soil varying with depth

Fig. 6 Profiles of electrical resistivity in the wells, alongside the lithology and groundwater levels in the wells

Table 2 Measured electrical conductivity (EC) at different groundwater and river sampling sites

Well ID	EC (µS/cm)	Measurement date
Groundwater		
a1	135	14 Dec. 2018
a1	160	6 Jun. 2019
a2	146	14 Dec. 2018
a2	167	6 Jun. 2019
a3	160	14 Dec. 2018
a3	185	6 Jun. 2019
a4	185	14 Dec. 2018
a4	206	6 Jun. 2019
River water		
a5	205	14 Dec. 2018
a5	313	6 Jun. 2019

Electrical resistivity tomography validation with hydrogeology

For validation of the ERT results with measurements of the groundwater level, the electrical resistivity values at a horizontal distance of 180 m, at different depths, were extracted along each ERT line (lines 1–4 in Fig. 1c). The electrical resistivity values along each ERT line were averaged across the same depths to eliminate lithology anisotropy.

The distributive features of the vadose zone and the shallow and middle aquifer layers were determined by comparing the corresponding electrical resistivity values. The profiles of electrical resistivity values and lithology against depth are shown in Fig. 6.
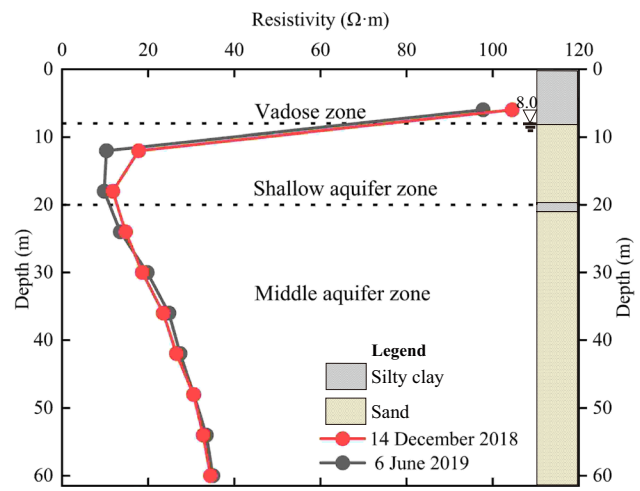
The lithology of the top *resistivity zone* or *unit* (depth 0–8 m) is silty clay characterized by an uneven electrical resistivity distribution. Previously, it was reported that the top unit was characterized by an uneven electrical resistivity distribution indicating vegetation–soil interaction (Alamry et al. 2017). The top unit was characterized by variable electrical resistivity associated with changes in water saturation caused by evapotranspiration (Tesfaldet and Puttiwongrak 2019). The vadose zone is inferred at depths of 0–8 m according to the electrical resistivity distribution and the water table of the shallow aquifer at a depth of 8 m.

Below the vadose zone (at depths of 8–20 m) is the middle unit; the lithology of the middle unit is sand and the corresponding electrical resistivity values range from 10 to 70 Ω·m. The electrical resistivity values below 25 Ω·m can be interpreted as a saturated aquifer zone (Pan and Liu 2014). The middle unit is characterized by a major electrical resistivity change among two sampling dates. The middle unit displays a uniform electrical resistivity change between the survey dates, and combined with the uneven electrical resistivity distribution of the top unit, this indicates a change in the water content of the middle unit (Alamry et al. 2017). The shallow aquifer is inferred at depths of 8–20 m according to the electrical resistivity distribution and the water table at a depth of 8 m. It is further inferred that the shallow aquifer is formed by scouring during large flood events because of channel convergence (Cendón et al. 2010). At the base of the shallow aquifer is a unit of silty sand. The electrical resistivity does not notably change between the dry and wet seasons, so this unit is assumed to be the middle aquifer. Compared to the electrical resistivity values of the shallow aquifer,

there is a significant increasing trend in the middle aquifer. This increase in electrical resistivity is consistent in ERT lines 1–3. However, the electrical resistivity values in ERT line 4 are potentially overestimated because the electrical resistivity values were averaged across the same depths to eliminate lithology anisotropy.

Results

Water-table variations

Figure 7 shows the variation of the water level of the Yellow River (a5) and variations of the water table of the shallow aquifer (wells a1, a2, a3, and a4) over time from December 2018 to June 2019.

The water levels in wells a1, a2, and a3 did not change significantly from April to May 2019, indicating that the larger distance of 3.45 km from the Yellow River makes recharge more difficult. The shallow aquifer represented by well a4 shows a brief decline of the water table from April to May 2019, as a result of groundwater pumping for irrigation, followed by a swift recovery. At a distance of 1.2 km from the Yellow River, the water level in well a4 dropped 1.4 m, taking 5 days to recover; well a4 recovered quickly because of its proximity to the Yellow River and the associated ease of recharge. It is reported that this study region has a shallow water table because of lateral seepage from the Yellow River and vertical recharge from surface irrigation (Shen et al. 2011). Generally, the greatest use of Yellow River irrigation water takes place in the lower reaches of Henan province, which plays a significant role in food production in China (Chen et al. 2013; Mingzhou et al. 2007;

Wang et al. 2016). It is reported that the mean annual water application in the irrigation districts along the lower Yellow River was up to 481 mm in 2009 (Liu et al. 2009). The study region reported in this paper is located in the Yellow River irrigation region, which is a key region for food production, where vast agricultural fields of staple crops are cultivated (Deng et al. 2006; Nakayama 2011).

It is also noted that high groundwater levels occur in the center of line 2 and low groundwater levels are found on both sides (Fig. 8b), which is thought to be caused by architecture usage (i.e., caused by the effects of subsurface architecture on groundwater flow).

Electrical imaging

Resistivity values were used to determine the resistivity distribution for the following three resistivity units: the vadose layer of the top unit, the shallow aquifer layer of the middle unit, and the middle aquifer layer of the bottom unit in both dry and wet seasons.

Based on the ERT inversion results (Fig. 8), the top unit is assumed to be a vadose layer of a wide range of resistivity values (21–221 Ω-m). The resistivity of the top unit is represented by green and red areas in Fig. 8. The top unit is a silty layer in the high floodplain and sandy silt in the low floodplain with an average thickness of 8 m. Most resistivity values of the top unit are high because of dryness. This unit indicates a subtle spatiotemporal variation in the resistivity distribution over different seasons. The resistivity values decreased which may be because of irrigation during the dry season, which is further supported by the top unit of line 2, extending 144–234 m in the x-direction, being a vadose zone in the high floodplain (Fig. 8b,f). However, the resistivity values of this top unit remain high throughout the entire transition season in line 4 in the low floodplain (Fig. 8d,h) which may be because of the location of line 4 in a sandy silt area of the low floodplain.

Below the top unit, the resistivity values of the middle unit decline to values of 10–70 Ω-m. This phenomenon occurs at a depth of approximately 11 m which is marked with blue and light blue color in Fig. 8. This blue zone has lower resistivity values than both the lower and upper sections. According to the geological cross-section along A–B and resistivity values of the middle unit, this middle unit is assumed to be the shallow aquifer layer. This decline in the resistivity values in the high floodplain (lines 1, 2, and 3) may be attributed to rainfall. The water levels of wells a1, a2 and a3 do not change significantly (see section 'Water-table variations'), indicating that the locations of lines 1–3 are hardly recharged from the Yellow River. This decline in the resistivity values occurs in the top unit at a distance of 150–240 m in line 2 (Fig. 8b). The extent of the low electrical resistivity indicates vertical water movement in
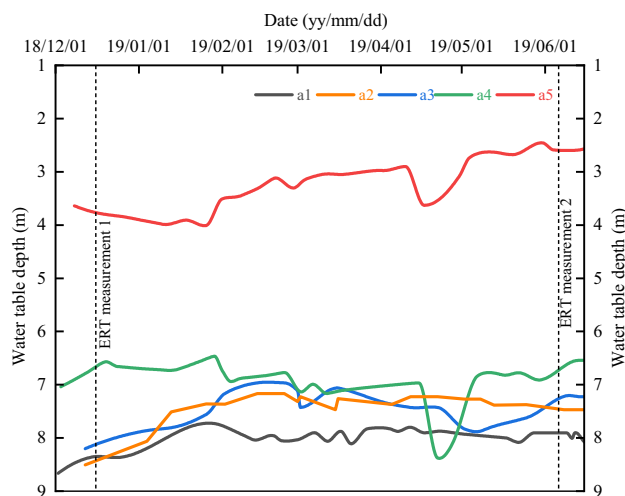

Fig. 7 Water levels in the four wells of the shallow aquifer and water level of the Yellow River measured in well a5

Fig. 8 Comparison of the inversion results for the four ERT lines on 14 December 2018 (**a** line 1, **b** line 2, **c** line 3, and **d** line 4), and 6 June 2019 (**e** line 1, **f** line 2, **g** line 3, and **h** line 4). The dotted black arrows of line 4 indicate the direction of the shallow groundwater flow
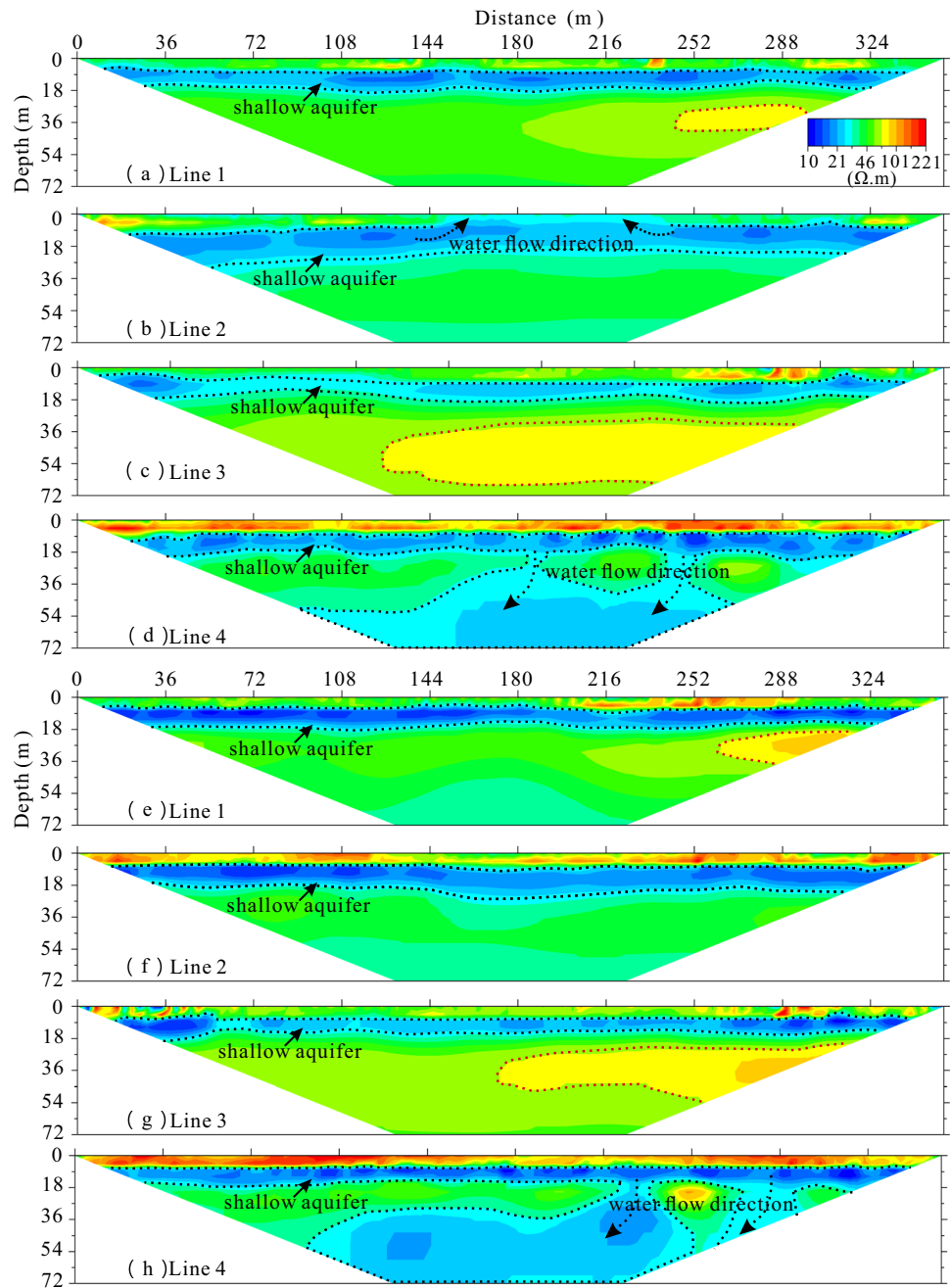
the top unit. Similarly, there is a local decrease in electrical resistivity irregularly distributed from distance 0–36 m and at 9 m depth in line 3 (Fig. 8g), indicating vertical water movement. However, the pattern of rainfall recharge to the shallow aquifer is different in lines 1–3, which will be discussed in detail later. Time-lapse ERT imaging also demonstrates a decline in resistivity values in the high floodplain attributable to rainfall, which will be discussed in the next section 'Time-lapse electrical resistivity tomography'. The blue color of the middle unit in Fig. 8 is laterally discontinued in the high floodplain. Compared to the high floodplain,

the resistivity values of the low floodplain (line 4) in the wet season (Fig. 8d) are lower than in the dry season (Fig. 8h). Furthermore, the blue color of the middle unit shows more connection laterally in the wet season. Because of the river recharge effect, the groundwater level is significantly higher where line 4 gets closer to the river (located at a distance from the river of 1.2 km), where more Yellow River water seeps into the shallow aquifer. Measurement data show low resistivity values during the dry season in the middle unit, whereas during the wet season, this saturated layer was significantly enlarged vertically and laterally in line 4.

The bottom unit is denoted by anomalies in resistivity values ranging from 30 to 101 Ω-m (Fig. 8). Integrating the geological cross-section along A–B with resistivity value variations of the bottom unit, the bottom unit is believed to be the middle aquifer. While the resistivity values of the bottom unit are mostly stable, Fig. 8 shows resistivity anomalies. In Fig. 8a, along line 1, the high-resistivity anomaly zone is colored yellow and demarcated by a red dotted line. The high-resistivity anomaly zone is located 243 m from the end of the ERT line and vertically from depths 26–40 m. This anomaly is related to the middle aquifer. During the wet season, as depicted in Fig. 8e, this anomaly zone of line 1 decreased in size because of the enrichment in the ionic concentration of the groundwater (Clément et al. 2009). There is little change in the resistivity anomaly zones of line 2 during dry and wet seasons. Line 3 showed similar phenomena to line 1 and is demarcated by a red dotted line in Fig. 8c,g. The yellow anomaly zone in the dry season was evident from 355 to 126 m from the end of line 3, and vertically from depths 32 to 65 m (Fig. 8g). However, in the wet season, this yellow anomaly zone of line 3 seems to diminish, from 355 to 141 m from the end, and vertically from 25 to 46 m. As shown in Fig. 8d, in the dry season, the low-resistivity anomaly zone of line 4 is located at 90 to 252 m and vertically from 45 to 72 m. In the wet season, the low-resistivity anomaly zone remains laterally identical, with a vertical extension from 31 to 72 m (Fig. 8h), but its low resistivity is even lower. Furthermore, the hydraulic connection between the shallow aquifer and middle aquifer of line 4 can be identified by low-resistivity anomalies, which are marked by the black arrows in Fig. 8d,h; however, the locations of the black arrows are inconsistent in Fig. 8d,h. This inconsistency is associated with artifacts caused by the relocation of electrodes and bad datum points—i.e., caused by high contact resistance between the electrode and ground or faulty electrodes.

Time-lapse electrical resistivity tomography

Time-lapse inversion analysis of the ERT data was performed using EarthImager 2D. The time-lapse ERT data, collected in December 2018, served as the base model for the following data collection, which occurred in June 2019. Finally, the inversion models calculated a percentage difference between the base and monitoring resistivity values.

The results of the time-lapse ERT inversion of lines 1–4 are shown in Fig. 9, representing the percentage change in resistivity values from December 14, 2018, to June 6, 2019. The red or blue colors in Fig. 9 indicate increasing or decreasing resistivity, respectively. Throughout the monitoring period, resistivity variations show large amplitude changes from –100 to 100%, equal to a decrease to half or an increase to double the initial resistivity, respectively.

In Fig. 9a, along line 1, the resistivity decrease is attributed to the preferential recharge zones located between 216 and 306 m. The more conductive zones allow more flow and become preferential flow paths (Nimmo 2021). Similarly, the consistency of these preferential recharge zones—water enters and exits quickly (Wallin et al. 2013)—can also be found in line 3 (Fig. 9c). In Fig. 9c, preferential recharge zones are demarcated by the black arrows at 18, 90, 279, and 315 m in line 3 (Fig. 9c); however, in Fig. 9b, along line 2, the resistivity decrease is attributed to the plug (slow) recharge zones located from 108 to 354 m. The recharge in line 2 in the vadose zone is mainly controlled by slowly moving wetting fronts. The plug flow is faster than the preferential flow; furthermore, the preferential flow often occurs through the entire aquifers and can extend far lower (Nimmo 2021) (for instance lines 1 and 3). Different sediments lead to preferential or plug recharge in the vadose zone. Preferential flow occurs in the vadose zone due to different hydraulic processes, often associated with obvious flowpaths such as fractures or biopores (De Carlo et al. 2021), but also in supposedly homogeneous materials (Gjettermann et al. 1997; Green et al. 2005).

In Fig. 9d, along line 4, up to a distance of 355 m, resistivity values are strong and clearly reduced from –100 to –50%, represented by blue color (demarcated by the black dotted line). The strong resistivity decrease extends from the top unit to the middle unit of line 4. Resistivity decrease implies water infiltration through the top unit and the middle unit during the wet season. The percentage variations of resistivity over time provide an indirect indication of the amount of water contained in the pore space. The time-lapse ERT on line 4 at both times indicates that more water flux is coming from the Yellow River to the shallow aquifer, and the Yellow River is the preferred recharge zone of this aquifer. The preferential recharge zones are regularly connected to the shallow aquifer throughout line 4, forming the preferred flow. The nature of the preferred recharge zone demonstrates the hydraulic heterogeneity of the silty clay and sand deposit.

Hence, it can be inferred that the shallow aquifer recharge pattern differs between the high and low floodplain. Geologically, ERT line 4 is located in the low floodplain, while the remaining three ERT lines are located in the high floodplain, indicating that in the high floodplain, the recharge of the top unit (i.e., the vadose zone) is controlled by slow drainage of the wetting fronts as indicated by the time-lapse ERT (Fig. 9a–c). In addition, the time-lapse ERT shows a strong seasonal resistivity variation in the top unit, indicating water infiltration during the wet season. This relationship suggests that the recharge of the shallow aquifer depends on the precipitation (mean) in the study area; however, in the low floodplain, the recharge of the shallow aquifer not only depends on the precipitation but also on the Yellow River.

Fig. 9 Percentage change in resistivity between the two distinct seasons for the four different lines in the period from 14 December 2018, to 6 June 2019: **a** line 1, **b** line 2, **c** line 3, **d** line 4. The red-colored areas indicate increases in electrical resistivity, whereas the blue-colored areas indicate decreases in resistivity. The black arrows of line 3 indicate preferential recharge zones
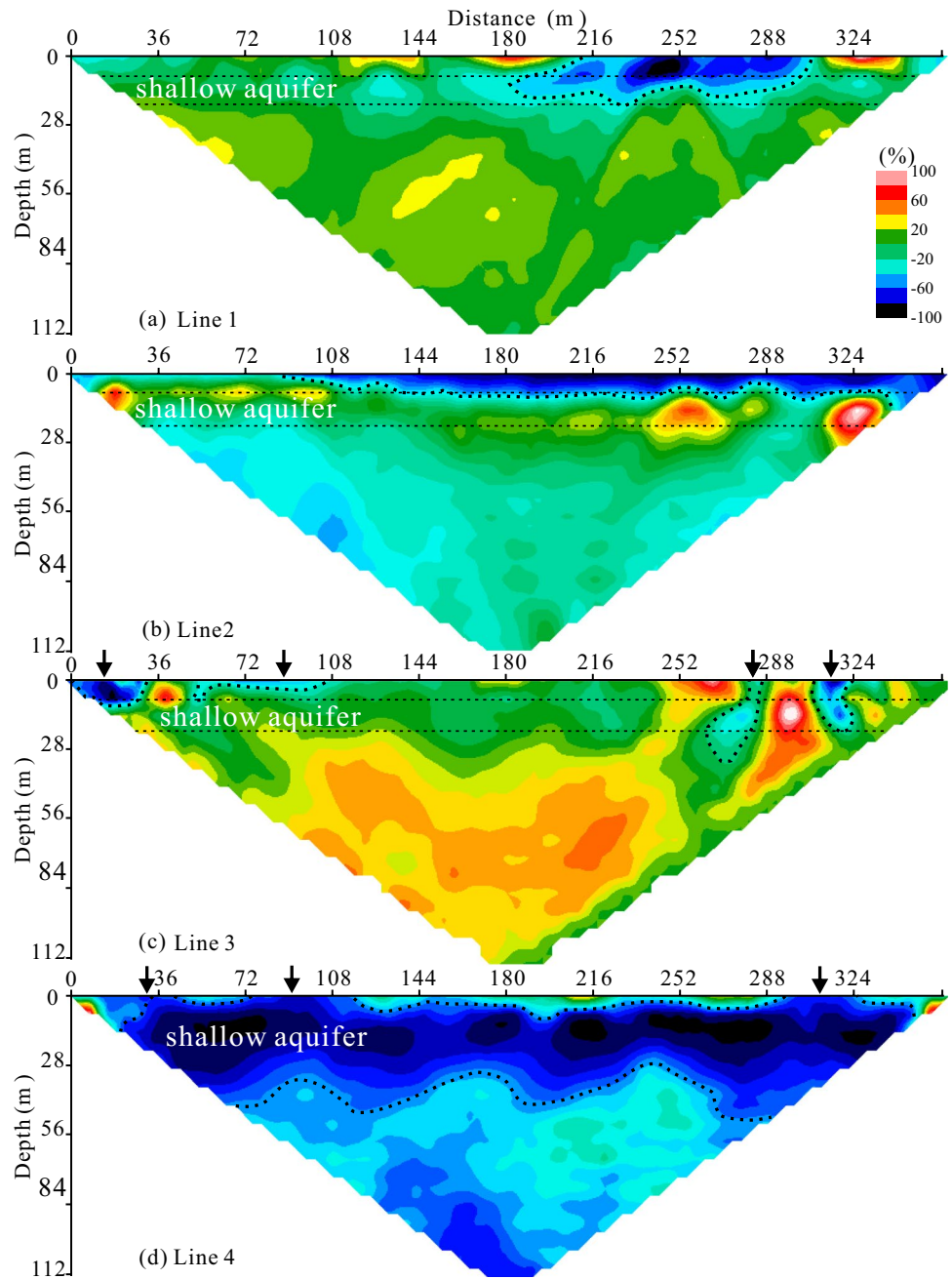
Discussion

The fluctuation of groundwater level in a monitoring well is caused by groundwater recharge or discharge. The water table rises in a shallow aquifer as a response to variation in storage due to water infiltration (Healy and Cook 2002). On the other hand, water-table falls indicate a discharge from the shallow aquifer through pumping. Monitoring of the water-table fluctuation provides information on the dynamics of the recharge on a local scale. Previous studies have shown that this area has a shallow water table because of lateral seepage from the Yellow River and vertical recharge from

surface irrigation and rainfall (Shen et al. 2011). Compared with 12.95 mm in December 2018, the mean precipitation in June 2019 was 115.51 mm. These data suggest that groundwater is partly recharged from recent local precipitation via vertical seepage. This result is confirmed by the fluctuation of the water table and ERT results—for instance, the groundwater level depths of wells a1–a4 were 8.6, 8.5, 8.2, and 6.6 m on December 14, 2018, then reached 7.9, 7.5, 7.2, and 6.7 m on June 6, 2019 during the wet season. The relationship between the fluctuation of the water table and rainfall suggests the dependency of recharge on the precipitation (mean) in the study area (Kotchoni et al. 2018). This relationship

further implies significant variations in ERT results during the onset of the wet season, as anticipated. Due to the large vertical scale of Fig. 8 and the slight variation in groundwater level at different locations (ERT lines 1–4), there was no noticeable change in the groundwater depth of the shallow aquifers on the four survey lines. The water level depths of the shallow aquifer of lines 1–4 were 8.6, 8.5, 8.2, and 7.2 m, respectively, in the dry season. Conversely, the water table of the shallow aquifer rose in the wet season, and the water level depths of the shallow aquifer of lines 1–4 were 7.9, 7.5, 7.2, and 6.7 m, respectively. In contrast, the water table in line 4 was comparatively low during the dry and wet seasons and, additionally, was very close to the level of the Yellow River. The water level of the Yellow River was 3.75 m below ground level on December 14, 2018, then reached a depth of 2.6 m on June 6, 2019. Overall, groundwater recharge decreased with an increase in the distance from the Yellow River (Zhao and Li 2017), and this result is confirmed by the recovery efficiency of the water levels in wells a1–a4 (section 'Water-table variations') after the water table drops. Previous studies have shown that the peak of irrigation in the lower reaches of the Yellow River occurred in June and July, during which the irrigation consumption was relatively large (Xiao et al. 2022), and field seepage and surface runoff had the strongest influence (Liu et al. 2017).

The reduced resistivity of the shallow aquifer of line 4 in the low floodplain is most likely caused by the influx of river water with lower resistance. The water level of the Yellow River (a5) was always higher than that in well a4 in the low floodplain. Furthermore, responding to the water level of the Yellow River, the water level in well a4 fluctuated significantly, showing that the shallow aquifer is mainly recharged by river influx. However, the water levels of wells a1, a2, and a3 in the high floodplain remained relatively constant compared to that of well a4 and showed minimal reaction to the variation of the water level of the Yellow River. Well a3 was located at a distance of 3.45 km from the Yellow River and its water level measurements can be used as a reference for a water table that is unaffected by river water intrusion. The time-lapse ERT results are further corroborated by variations in resistivity of the shallow aquifer, as shown in Fig. 9. Resistivity variations from the dry to the wet season are much greater in line 4 than in lines 1, 2, and 3. The resistivity of the shallow aquifer and the vadose zone in line 4 decreased by 100%; and in addition, there were significant reductions of resistivity in lines 1, 2, and 3 in the vadose zone (Fig. 9). However, in Fig. 9c, an increase in resistivity for line 3 is shown at 252–270 m and 288–306 m in the vadose zone, and, there is also an increase in resistivity from 108 to 252 m in the middle aquifer. The increase in resistivity is associated with a time-lapse inversion artifact caused by a moisture contrast between the dry and wet season. The inversion artifacts are false results caused by the

inversion model's incapability to fit the contrasting electrical resistivity values' time-lapse inversion (Miller et al. 2008). Hydrological and geophysical data showed that the Yellow River always recharges the shallow aquifer in the floodplain, whereas further removed from the shallow aquifer surrounding the Yellow River, the influence of the Yellow River recharge decreases, and the influence of recharge by precipitation becomes more pronounced. The reasons are as follows. First of all, where groundwater recharge is dominated by infiltration from the Yellow River, the recharge rate of river infiltration slows down further away from the river. Therefore, the time lag and magnitude of difference between the groundwater levels and river stage increase with increasing distance from the Yellow River. Secondly, the transfer of water and sand from Xiaolangdi Reservoir makes the variation of the Yellow River water level smaller, and the intensity of lateral seepage recharge to the shallow aquifer is smaller; therefore, there is very little variation in the shallow-aquifer groundwater level. Thirdly, large-scale regional recharge of groundwater is by atmospheric precipitation, resulting in a smoothing of the groundwater level dynamics. Lastly, the farther away from the Yellow River, the more limited the Yellow River's measured seepage range and, thus, its ability to recharge groundwater lessens.

Resistivity changes between the dry and wet seasons are much larger for line 4 than for lines 1, 2, or 3. Based on Archie's law (Archie 1942), $\rho_b = a\rho_f\varphi^m S^n$, where a is a dimensionless fitting parameter representing tortuosity, m is the cementation factor, φ is the porosity, n is a model parameter, and S is the saturation. The bulk electrical resistivity (ρ_b) is largely determined by pore-water resistivity, which is controlled by the concentration of dissolved solids in the water, as well as water saturation, porosity, and clay content (de Jong et al. 2020; McLachlan et al. 2017; Mézquita González et al. 2020). Hence, it can be inferred that the degree of water saturation and concentration of dissolved solids (salinity) differ between the four locations. One can relate the electrical resistivity to water saturation or dissolved solids using a petrophysical transformation. Previous studies have shown that electrical resistivity decreases with increasing concentration of dissolved solids (salinity) and increasing water saturation (Coscia et al. 2012; De Carlo et al. 2020; Johnson et al. 2015); however, the effects of water saturation and salinity on the electrical resistivity are different in the vadose zone compared with the aquifer. The ERT method is particularly useful for studies on hydrological processes in the near-surface because of the high correlation between water saturation and electrical resistivity in the vadose zone (Binley et al. 1996, 2015; Daily et al. 1992; Michot et al. 2003; Revil et al. 2012); therefore, it can be inferred that the degree of saturation differs among the floodplains in the vadose zone. However, below the depth of 8 m, assuming other factors affecting electrical resistivity (porosity, clay content, and

water saturation) of the shallow and middle aquifers remain constant, an increase in electrical resistivity from the time-lapse ERT images can be solely attributed to the migration of dissolved solids (salinity). It can also be proved that, in the high floodplain, recharge of the shallow aquifer is controlled by precipitation, as indicated by the time-lapse ERT results (Fig. 9)—for instance, along lines 1–3, the decrease of electrical resistivity in the vadose zone is attributed to the preferential recharge zones at 216 and 306 m in line 1, 90 and 355 m in line 2, and 279 and 315 m in line 3 (Fig. 9). However, in the low floodplain, the recharge of the shallow aquifer not only depends on rainfall but also on the Yellow River (Figs. 8 and 9)—for instance, along line 4, the electrical resistivity decreased at 36, 90, and 306 m in the vadose zone and the shallow aquifer (Fig. 9). The result is further confirmed by water level variations of the Yellow River and in the wells a1–a4. The water table of the shallow aquifer (wells a1–a3) did not change as the water level of the Yellow River decreased from April to May 2019, indicating that the larger distance of 3.45 km away from the Yellow River (line 3) complicated the recharge of the shallow aquifer. However, at a distance of 1.2 km (line 4), the shallow aquifer was easily recharged by the Yellow River (Fig. 7).

A hydraulic connection is inferred between the shallow aquifer and the middle aquifer. The groundwater of the shallow aquifer flows towards the middle aquifer according to line 4 (Fig. 8d,h) at a distance of 1.2 km from the Yellow River. At distances of 90–252 m, the groundwater in the shallow aquifer of line 4 with low resistivity (demarcated by black dotted lines) tends to flow to the middle aquifer (indicated by black arrows in Fig. 8d,h). At a distance of 1.2 km from the Yellow River, the water level in well a4 is always below the water level of the Yellow River; furthermore, the water table fell by 1.3 m due to the effects of subsurface architecture on groundwater flow and it took 5 days to recover. This indicates that the Yellow River recharges the shallow aquifer in line 4. The water level of the Yellow River in line 4 rose by 1.2 m from early December 2018 (during the dry season) to early June 2019 (during the wet season). The low-resistivity zone extends vertically from 45 to 31 m depth (black dotted lines in Fig. 8d,h). This implies that the groundwater of the shallow aquifer flows to the middle aquifer under high river water levels. As shown by Yan (2018), in this study region, the middle aquifer is hydraulically connected to the shallow aquifer.

Conclusions

A combination of ERT with data from hydrological wells was used to identify the recharge characteristics between the Yellow River and its adjacent shallow aquifer. Marked spatiotemporal variations were found both in the wet and dry seasons. The results obtained from two types of resistivity data (ERT and time lapse ERT) emphasize the importance of nondestructive investigations related to hydrogeological engineering projects for water resource utilization and resource protection.

The interpreted sections along four ERT lines have helped to delineate three significant hydrogeological units in the study area—namely the vadose zone, shallow aquifer, and middle aquifer (from shallow to deep). These zones correspond to a higher-resistive layer of silty sand (21–221 Ω-m) with an average thickness of 8 m, a lower-resistive layer of saturated sand (10–70 Ω-m) with an average thickness of 11 m, and a medium-resistive layer of saturated sand (30–101 Ω-m) with an average thickness of 45 m. Compared with the dry season, the resistivity values of all lines decrease during the wet period, which shows that both river water and rainfall flow into the shallow aquifer and then recharge the middle aquifer as a result of seepage from several preferential flow channels (probably the sedimentary discontinuity zone of the riverbed).

Based on time-lapse ERT images of these lines, the resistivity value of line 4 located in the low floodplain shows a decreasing tendency. Increasing resistivity value in the high floodplain occurs in other ERT lines away from the river. Different recharge patterns occur in different locations within various territorial units of the floodplain, even in the same season. The joint use of ERT and monitoring wells data is more effective than drilling for the in situ identification of groundwater infiltration paths and recharge characteristics associated with high-density surveys. This paper provides a reference method for the selection of locations suitable for stations to be used for the exploitation of groundwater resources.

Declarations

References

Acworth RI, Timms WA (2003) Hydrogeological investigation of mud-mound springs developed over a weathered basalt aquifer on the Liverpool Plains, New South Wales, Australia. Hydrogeol J 11:659–672. https://doi.org/10.1007/s10040-003-0278-0

Alamry AS, van der Meijde M, Noomen M, Addink EA, van Benthem R, de Jong SM (2017) Spatial and temporal monitoring of soil moisture using surface electrical resistivity tomography in

Mediterranean soils. CATENA 157:388–396. https://doi.org/10.1016/j.catena.2017.06.001

Amabile A, de Carvalho Faria Lima Lopes B, Pozzato A, Benes V, Tarantino A (2020) An assessment of ERT as a method to monitor water content regime in flood embankments: the case study of the Adige River embankment. Phys Chem Earth, Parts A/B/C 120. https://doi.org/10.1016/j.pce.2020.102930

Archie GE (1942) The electrical resistivity log as an aid in determining some reservoir characteristics. Energy 146:54–62. https://doi.org/10.2118/942054-G

Binley A (2015) Tools and techniques: electrical methods. In: Schubert G (ed) Treatise on geophysics, 2nd edn. Elsevier, Amsterdam, pp 233–259

Binley A, Henry-Poulter S, Shaw B (1996) Examination of solute transport in an undisturbed soil column using electrical resistance tomography. Water Resour Res 32:763–769. https://doi.org/10.1029/95WR02995

Binley A, Ullah S, Heathwaite AL, Heppell C, Byrne P, Lansdown K, Trimmer M, Zhang H (2013) Revealing the spatial variability of water fluxes at the groundwater–surface water interface. Water Resour Res 49:3978–3992. https://doi.org/10.1002/wrcr.20214

Binley A, Hubbard SS, Huisman JA, Revil A, Robinson DA, Singha K, Slater LD (2015) The emergence of hydrogeophysics for improved understanding of subsurface processes over multiple scales. Water Resour Res 51:3837–3866. https://doi.org/10.1002/2015WR017016

Cardenas MB, Wilson JL, Zlotnik VA (2004) Impact of heterogeneity, bed forms, and stream curvature on subchannel hyporheic exchange. Water Resour Res 40:W08307. https://doi.org/10.1029/2004WR003008

Cardenas MB, Zamora PB, Siringan FP, Lapus MR, Rodolfo RS, Jacinto GS, San Diego-McGlone ML, Villanoy CL, Cabrera O, Senal MI (2010) Linking regional sources and pathways for submarine groundwater discharge at a reef by electrical resistivity tomography, 222Rn, and salinity measurements. Geophys Res Lett 37:L16401. https://doi.org/10.1029/2010GL044066

Cendón DI, Larsen JR, Jones BG, Nanson GC, Rickleman D, Hankin SI, Pueyo JJ, Maroulis J (2010) Freshwater recharge into a shallow saline groundwater system, Cooper Creek floodplain, Queensland, Australia. J Hydrol 392:150–163. https://doi.org/10.1016/j.jhydrol.2010.08.003

Chen B, Ouyang Z, Sun Z, Wu L, Li F (2013) Evaluation on the potential of improving border irrigation performance through border dimensions optimization: a case study on the irrigation districts along the lower Yellow River. Irrig Sci 31:715–728. https://doi.org/10.1007/s00271-012-0338-0

Cheng Q, Chen X, Chen X, Zhang Z, Ling M (2011) Water infiltration underneath single-ring permeameters and hydraulic conductivity determination. J Hydrol 398:135–143. https://doi.org/10.1016/j.jhydrol.2010.12.017

Claerbout JF, Muir F (1973) Robust modeling with erratic data. Geophysics 38:826–844. https://doi.org/10.1190/1.1440378

Clément R, Descloitres M, Günther T, Ribolzi O, Legchenko A (2009) Influence of shallow infiltration on time-lapse ERT: experience of advanced interpretation. C R Geosci 341:886–898. https://doi.org/10.1016/j.crte.2009.07.005

Constantz J (2008) Heat as a tracer to determine streambed water exchanges. Water Resour Res 44, W00D10. https://doi.org/10.1029/2008WR006996

Coscia I, Greenhalgh SA, Linde N, Doetsch J, Marescot L, Gunther T, Vogt T, Green AG (2011) 3D crosshole ERT for aquifer characterization and monitoring of infiltrating river water. Geophysics 76:G49–G59. https://doi.org/10.1190/1.3553003

Coscia I, Linde N, Greenhalgh S, Günther T, Green A (2012) A filtering method to correct time-lapse 3D ERT data and improve imaging of natural aquifer dynamics. J Appl Geophys 80:12–24. https://doi.org/10.1016/j.jappgeo.2011.12.015

Daily W, Ramirez A, LaBrecque D, Nitao J (1992) Electrical resistivity tomography of vadose water movement. Water Resour Res 28:1429–1442. https://doi.org/10.1029/91WR03087

De Carlo L, Battilani A, Solimando D, Caputo MC (2020) Application of time-lapse ERT to determine the impact of using brackish wastewater for maize irrigation. J Hydrol 582. https://doi.org/10.1016/j.jhydrol.2019.124465

De Carlo L, Perkins K, Caputo MC (2021) Evidence of preferential flow activation in the vadose zone via geophysical monitoring. Sensors (Basel) 21. https://doi.org/10.3390/s21041358

De Jong SM, Heijenk RA, Nijland W, van der Meijde M (2020) Monitoring soil moisture dynamics using electrical resistivity tomography under homogeneous field conditions. Sensors (Basel) 20. https://doi.org/10.3390/s20185313

Deng X-P, Shan L, Zhang H, Turner NC (2006) Improving agricultural water use efficiency in arid and semiarid areas of China. Agric Water Manag 80:23–40. https://doi.org/10.1016/j.agwat.2005.07.021

Deng Y, Shi X, Xu H, Sun Y, Wu J, Revil A (2017) Quantitative assessment of electrical resistivity tomography for monitoring DNAPLs migration: comparison with high-resolution light transmission visualization in laboratory sandbox. J Hydrol 544:254–266. https://doi.org/10.1016/j.jhydrol.2016.11.036

Fleckenstein JH, Mniswonger RG, Fogg GE (2006) River–aquifer interactions, geologic heterogeneity, and low-flow management. Groundwater 44:837–852. https://doi.org/10.1111/j.1745-6584.2006.00190.x

Foster A, Trautz AC, Bolster D, Illangasekare T, Singha K (2021) Effects of large-scale heterogeneity and temporally varying hydrologic processes on estimating immobile pore space: a mesoscale-laboratory experimental and numerical modeling investigation. J Contam Hydrol 241:103811. https://doi.org/10.1016/j.jconhyd.2021.103811

Gelhar LW (1986) Stochastic subsurface hydrology from theory to applications. Water Resour Res 22:135S–145S. https://doi.org/10.1029/WR022i09Sp0135S

Gjettermann B, Nielsen KL, Petersen CT, Jensen HE, Hansen S (1997) Preferential flow in sandy loam soils as affected by irrigation intensity. Soil Technol 11:139–152. https://doi.org/10.1016/S0933-3630(97)00001-9

Green CT, Stonestrom DA, Bekins BA, Akstin KC, Schulz MS (2005) Percolation and transport in a sandy soil under a natural hydraulic gradient. Water Resour Res 41. https://doi.org/10.1029/2005WR004061

Harvey JW, Bencala KE (1993) The effect of streambed topography on surface–subsurface water exchange in mountain catchments. Water Resour Res 29(1):89–98. https://doi.org/10.1029/92wr01960

Healy RW, Cook PG (2002) Using groundwater levels to estimate recharge. Hydrogeol J 10:91–109. https://doi.org/10.1007/s10040-001-0178-0

Harvey J, Gooseff M (2015) River corridor science: hydrologic exchange and ecological consequences from bedforms to basins. Water Resour Res 51:6893–6922. https://doi.org/10.1002/2015WR017617

Hayley K, Bentley LR, Gharibi M, Nightingale M (2007) Low temperature dependence of electrical resistivity: implications for near surface geophysical monitoring. Geophys Res Lett 34(18). https://doi.org/10.1029/2007gl031124

Hermans T, Nguyen F, Robert T, Revil A (2014) Geophysical methods for monitoring temperature changes in shallow low enthalpy geothermal systems. Energies 7:5083–5118. https://doi.org/10.3390/en7085083

Hester ET, Cardenas MB, Haggerty R, Apte SV (2017) The importance and challenge of hyporheic mixing. Water Resour Res 53:3565–3575. https://doi.org/10.1002/2016WR020005

Hiscock KM, Grischek T (2002) Attenuation of groundwater pollution by bank filtration. J Hydrol 266:139–144. https://doi.org/10.1016/S0022-1694(02)00158-0

Johnson T, Versteeg R, Thomle J, Hammond G, Chen X, Zachara J (2015) Four-dimensional electrical conductivity monitoring of stage-driven river water intrusion: accounting for water table effects using a transient mesh boundary and conditional inversion constraints. Water Resour Res 51:6177–6196. https://doi.org/10.1002/2014wr016129

Kelly S, Murdoch L (2003) Measuring the hydraulic conductivity of shallow submerged sediments. Groundwater 41:431–439. https://doi.org/10.1111/j.1745-6584.2003.tb02377.x

Kiel BA, Bayani Cardenas M (2014) Lateral hyporheic exchange throughout the Mississippi River network. Nat Geosci 7:413–417. https://doi.org/10.1038/ngeo2157

Kim J-H, Yi M-J, Park S-G, Kim JG (2009) 4-D inversion of DC resistivity monitoring data acquired over a dynamically changing earth model. J Appl Geophys 68:522–532. https://doi.org/10.1016/j.jappgeo.2009.03.002

Kotchoni DOV, Vouillamoz J-M, Lawson FMA, Adjomayi P, Boukari M, Taylor RG (2018) Relationships between rainfall and groundwater recharge in seasonally humid Benin: a comparative analysis of long-term hydrographs in sedimentary and crystalline aquifers. Hydrogeol J 27:447–457. https://doi.org/10.1007/s10040-018-1806-2

Krause S, Blume T, Cassidy NJ (2012) Investigating patterns and controls of groundwater up-welling in a lowland river by combining fibreoptic distributed temperature sensing with observations of vertical hydraulic gradients. Hydrol Earth Syst Sci 16:1775–1792. https://doi.org/10.5194/hess-16-1775-2012

Kumar MD (2018) Does hard evidence matter in policy making the case of climate change and land use change? Water Policy Sci Pol 99-114. https://doi.org/10.1016/B978-0-12-814903-4.00006-3

Lautz LK, Siegel DI (2006) Modeling surface and ground water mixing in the hyporheic zone using MODFLOW and MT3D. Adv Water Resour 29:1618–1633. https://doi.org/10.1016/j.advwatres.2005.12.003

Levy J, Birck MD, Mutiti S, Kilroy KC, Windeler B, Idris O, Allen LN (2011) The impact of storm events on a riverbed system and its hydraulic conductivity at a site of induced infiltration. J Environ Manag 92:1960–1971. https://doi.org/10.1016/j.jenvman.2011.03.017

Liu Y, Wang L, Ni G, Cong Z (2009) Spatial distribution characteristics of irrigation water requirement for main crops in China. Trans CSAE 25:6–12. https://doi.org/10.3969/j.issn.1002-6819.2009.12.002

Liu L, Ma J, Luo Y, He C, Liu T (2017) Hydrologic simulation of a winter wheat–summer maize cropping system in an irrigation district of the Lower Yellow River Basin, China. Water 9. https://doi.org/10.3390/w9010007

Liu DS, Zhao J, Chen XB, Li YY, Weiyan SP, Feng MM (2018) Dynamic processes of hyporheic exchange and temperature distribution in the riparian zone in response to dam-induced water fluctuations. Geosci J 22(3):465–475. https://doi.org/10.1007/s12303-017-0065-x

Liu X, Shi C, Zhou Y, Gu Z, Li H (2019) Response of erosion and deposition of channel bed, banks and floodplains to water and sediment changes in the Lower Yellow River. China Water 11. https://doi.org/10.3390/w11020357

Loke MH (2004) Tutorial: 2-D and 3-D electrical imaging surveys. https://sites.ualberta.ca/~unsworth/UA-classes/223/loke_course_notes.pdf. Accessed November 2022

Loke MH, Barker RD (1996) Practical techniques for 3D resistivity surveys and data inversion. Geophys Prospect 44:499–523. https://doi.org/10.1111/j.1365-2478.1996.tb00162.x

Ludwig AL, Hession WC (2015) Groundwater influence on water budget of a small constructed floodplain wetland in the Ridge and Valley of Virginia, USA. J Hydrol: Region Stud 4:699–712. https://doi.org/10.1016/j.ejrh.2015.10.003

Marzadri A, Dee M, Tonina D, Bellin A, Tank J (2017) Role of surface and subsurface processes in scaling N$_2$O emissions along riverine networks. Proc Natl Acad Sci 114:201617454. https://doi.org/10.1073/pnas.1617454114

Maurer H, Friedel S, Jaeggi D (2009) Characterization of a coastal aquifer using seismic and geoelectric borehole methods. Near Surf Geophys 7:353–366. https://doi.org/10.3997/1873-0604.2009014

McLachlan PJ, Chambers JE, Uhlemann SS, Binley A (2017) Geophysical characterisation of the groundwater–surface water interface. Adv Water Resour 109:302–319. https://doi.org/10.1016/j.advwatres.2017.09.016

Mézquita González JA, Comte J-C, Legchenko A, Ofterdinger U, Healy D (2020) Quantification of groundwater storage heterogeneity in weathered/fractured basement rock aquifers using electrical resistivity tomography: sensitivity and uncertainty associated with petrophysical modelling. J Hydrol. https://doi.org/10.1016/j.jhydrol.2020.125637

Michot D, Benderitter Y, Dorigny A, Nicoullaud B, King D, Tabbagh A (2003) Spatial and temporal monitoring of soil water content with an irrigated corn crop cover using surface electrical resistivity tomography. Water Resour Res 39. https://doi.org/10.1029/2002WR001581

Miller CR, Routh PS, Brosten TR, McNamara JP (2008) Application of time-lapse ERT imaging to watershed characterization. Geophysics 73:G7–G17. https://doi.org/10.1190/1.2907156

Mingzhou Q, Jackson RH, Zhongjin Y, Jackson MW, Bo S (2007) The effects of sediment-laden waters on irrigated lands along the lower Yellow River in China. J Environ Manag 85:858–865. https://doi.org/10.1016/j.jenvman.2006.10.015

Musgrave H, Binley A (2011) Revealing the temporal dynamics of subsurface temperature in a wetland using time-lapse geophysics. J Hydrol 396(3-4):258–266. https://doi.org/10.1016/j.jdydrol.2010.11.008

Nakayama T (2011) Simulation of the effect of irrigation on the hydrologic cycle in the highly cultivated Yellow River Basin. Agric For Meteorol 151:314–327. https://doi.org/10.1016/j.agrformet.2010.11.006

Nguyen F, Kemna A, Antonsson A, Engesgaard P, Kuras O, Ogilvy R, Gisbert J, Jorreto S, Pulido-Bosch A (2009) Characterization of seawater intrusion using 2D electrical imaging. Near Surf Geophys 7:377–390. https://doi.org/10.3997/1873-0604.2009025

Nijland W, van der Meijde M, Addink EA, de Jong SM (2010) Detection of soil moisture and vegetation water abstraction in a Mediterranean natural area using electrical resistivity tomography. Catena 81:209–216. https://doi.org/10.1016/j.catena.2010.03.005

Nimmer RE, Osiensky JL, Binley AM, Sprenke KF, Williams BC (2007) Electrical resistivity imaging of conductive plume dilution in fractured rock. Hydrogeol J 15:877–890. https://doi.org/10.1007/s10040-007-0159-z

Nimmo JR (2021) The processes of preferential flow in the unsaturated zone. Soil Sci Soc Am J 85:1–27. https://doi.org/10.1002/saj2.20143

Nyquist JE, Freyer PA, Toran L (2008) Stream bottom resistivity tomography to map ground water discharge. GroundWater 46:561–569. https://doi.org/10.1111/j.1745-6584.2008.00432.x

Ogilvy RD, Meldrum PI, Kuras O, Wilkinson PB, Chambers JE, Sen M, Pulido-Bosch A, Gisbert J, Jorreto S, Frances I, Tsourlos P (2009) Automated monitoring of coastal aquifers with electrical resistivity tomography. Near Surf Geophys 7:367–375. https://doi.org/10.3997/1873-0604.2009027

Pan K, Liu J (2014) A parameter identification problem for spontaneous potential logging in heterogeneous formation. J Inverse Ill-posed Prob 22:357–373. https://doi.org/10.1515/jip-2012-0066

Peng J, Chen S, Dong P (2010) Temporal variation of sediment load in the Yellow River basin, China, and its impacts on the lower

reaches and the river delta. Catena 83:135–147. https://doi.org/10.1016/j.catena.2010.08.006

Rein A, Hoffmann R, Dietrich P (2004) Influence of natural time-dependent variations of electrical conductivity on DC resistivity measurements. J Hydrol 285(1–4):215–232. https://doi.org/10.1016/j.jhydrol.2003.08.015

Revil A, Cathles LM, Losh S, Nunn JA (1998) Electrical conductivity in shaly sands with geophysical applications. J Geophys Res Solid Earth 103(B10):23925–23936. https://doi.org/10.1029/98jb02125

Revil A, Karaoulis M, Johnson T, Kemna A (2012) Review: Some low-frequency electrical methods for subsurface characterization and monitoring in hydrogeology. Hydrogeol J 20:617–658. https://doi.org/10.1007/s10040-011-0819-x

Satter GS, Keramat M (2016) Deciphering transmissivity and hydraulic conductivity of the aquifer by vertical electrical sounding (VES) experiments in Northwest Bangladesh. Appl Water Sci 6(1):35–45. https://doi.org/10.1007/s13201-014-0203-9

Sebok E, Duque C, Engesgaard P, Boegh E (2015) Spatial variability in streambed hydraulic conductivity of contrasting stream morphologies: channel bend and straight channel. Hydrol Process 29:458–472. https://doi.org/10.1002/hyp.10170

Shen Y, Lei H, Yang D, Kanae S (2011) Effects of agricultural activities on nitrate contamination of groundwater in a Yellow River irrigated region. IAHS-AISH Publ. 348, pp 73–80. https://doi.org/10.1016/j.jhydrol.2011.07.036

Singha K, Gorelick SM (2006) Hydrogeophysical tracking of three-dimensional tracer migration: the concept and application of apparent petrophysical relations. Water Resour Res 42(6). https://doi.org/10.1029/2005wr004568

Singha K, Day-Lewis FD, Lane JW (2007) Geoelectrical evidence of bicontinuum transport in groundwater. Geophys Res Lett 34(12). https://doi.org/10.1029/2007gl030019

Singha K, Pidlisecky A, Day-Lewis FD, Gooseff MN (2008) Electrical characterization of non-Fickian transport in groundwater and hyporheic systems. Water Resour Res 4(4):1–14. https://doi.org/10.1029/2008WR007048

Singha K, Day-Lewis FD, Johnson T, Slater LD (2015) Advances in interpretation of subsurface processes with time-lapse electrical imaging. Hydrol Process 29:1549–1576. https://doi.org/10.1002/hyp.10280

Slater L, Binley A (2006) Synthetic and field-based electrical imaging of a zerovalent iron barrier: implications for monitoring long-term barrier performance. Geophysics 71:B129–B137. https://doi.org/10.1190/1.2235931

Storey RG, Howard KWF, Williams DD (2003) Factors controlling riffle-scale hyporheic exchange flows and their seasonal changes in a gaining stream: a three-dimensional groundwater flow model. Water Resour Res 39:1034. https://doi.org/10.1029/2002WR001367

Sutter E, Ingham M (2017) Seasonal saline intrusion monitoring of a shallow coastal aquifer using time-lapse DC resistivity traversing. Near Surf Geophys 15:59–73. https://doi.org/10.3997/1873-0604.2016039

Swanson TE, Cardenas MB (2010) Diel heat transport within the hyporheic zone of a pool-riffle-pool sequence of a losing stream and evaluation of models for fluid flux estimation using heat. Limnol Oceanogr 5:1741–1754. https://doi.org/10.4319/lo.2010.55.4.1741

Tesfaldet YT, Puttiwongrak A (2019) Seasonal groundwater recharge characterization using time-lapse electrical resistivity tomography in the Thepkasattri watershed on Phuket Island. Thailand Hydrol 6. https://doi.org/10.3390/hydrology6020036

Wallin EL, Johnson TC, Greenwood WJ, Zachara JM (2013) Imaging high stage river-water intrusion into a contaminated aquifer along a major river corridor using 2-D time-lapse surface electrical resistivity tomography. Water Resour Res 49:1693–1708. https://doi.org/10.1002/wrcr.20119

Wang W, Song X, Ma Y (2016) Identification of nitrate source using isotopic and geochemical data in the lower reaches of the Yellow River irrigation district (China). Environ Earth Sci 75:936. https://doi.org/10.1007/s12665-016-5721-3

Ward AS (2016) The evolution and state of interdisciplinary hyporheic research. WIREs Water 3:83–103. https://doi.org/10.1002/wat2.1120

Ward AS, Gooseff MN, Singha K (2010a) Imaging hyporheic zone solute transport using electrical resistivity. Hydrol Process 24:948–953. https://doi.org/10.1002/hyp.7672

Ward AS, Gooseff MN, Singha K (2010b) Imaging hyporheic zone solute transport using electrical resistivity. Hydrol Process 24(7):948–953. https://doi.org/10.1002/hyp.7672

Weatherill JJ (2015) Investigating the natural attenuation and fate of a trichloroethene plume at the groundwater-surface water interface of a UK lowland river. PhD Thesis, Keele University, Keele, England. https://eprints.keele.ac.uk/2339. Accessed November 2022

Wilkinson PB, Meldrum PI, Kuras O, Chambers JE, Ogilvy HRD (2010) High-resolution electrical resistivity tomography monitoring of a tracer test in a confined aquifer. J Appl Geophys 70(4):268–276. https://doi.org/10.1016/j.jappgeo.2009.08.001

Wohlfart C, Kuenzer C, Chen C, Liu G (2016) Social–ecological challenges in the Yellow River basin (China): a review. Environ Earth Sci 75. https://doi.org/10.1007/s12665-016-5864-2

Xiao D, Niu H, Guo F, Zhao S, Fan L (2022) Monitoring irrigation dynamics in paddy fields using spatiotemporal fusion of Sentinel-2 and MODIS. Agric Water Manag 263:107409. https://doi.org/10.1016/j.agwat.2021.107409

Xie Y, Batlle-Aguilar J (2017) Limits of heat as a tracer to quantify transient lateral river–aquifer exchanges. Water Resour Res 53(9):7740–7755. https://doi.org/10.1002/2017wr021120

Yan WF (2018) Recharge on the transformation between sulfer water and groundwater based on environmental environmental isotopes in the Yubei plain. China Univ Geosci. https://doi.org/10.27493/d.cnkigzdzy.2018.000019

Yang Z, Deng YP, Qian JZ, Ding R, Ma L (2021) Characterizing temporal behavior of a thermal tracer in porous media by time-lapse electrical resistivity measurements. Hydrogeol J. https://doi.org/10.1007/s10040-021-02307-1

Yeh T-CJ, Lee C-H, Hsu K-C, Illman WA, Barrash W, Cai X, Daniels J, Sudicky E, Wan L, Li G, Winter CL (2008) A view toward the future of subsurface characterization: CAT scanning groundwater basins. Water Resour Res 44. https://doi.org/10.1029/2007wr006375

Yu L (2002) The Huanghe (Yellow) River: a review of its development, characteristics, and future management issues. Cont Shelf Res 22:389–403. https://doi.org/10.1016/S0278-4343(01)00088-7

Zhang J, Song J, Long YG, Zhang Y, Zhang B, Wang Y, Wang YY (2017) Quantifying the spatial variations of hyporheic water exchange at catchment scale using the thermal method: a case study in the Weihe River. China Adv Meteorol 2017:8. https://doi.org/10.1155/2017/6159325

Zhao X, Li F (2017) Isotope evidence for quantifying river evaporation and recharge processes in the lower reaches of the Yellow River. Environ Earth Sci 76:123. https://doi.org/10.1007/s12665-017-6442-y

Zhou T, Huang MY, Bao J, Hou ZS, Arntzen E, Mackley R, Crump A, Goldman AE, Song XH, Xu Y, Zachara J (2017) A new approach to quantify shallow water hydrologic exchanges in a large regulated river reach. Water 9(9):703. https://doi.org/10.3390/w9090703